ISSN 0208-7774 TRIBOLOGIA 2/2023 p. 73–84
DOI: 10.5604/01.3001.0053.6126

Piotr SZCZYGLAK[*], Jerzy NAPIÓRKOWSKI[**], Mateusz SYDORCZYK[***]

AN EVALUATION OF THE EFFECT OF SILICA DUST ON BRAKE PAD WEAR

OCENA WPŁYWU ZAPYLENIA PYŁEM KWARCOWYM NA ZUŻYCIE KLOCKÓW HAMULCOWYCH

Key words: brake pads, wear, dust.

Abstract: The wear of brake pads exposed to silica dust was measured. A novel test stand was developed to analyse brake pads' wear exposed to silica dust. Brake pad wear was determined by measuring pad lining geometry and mass changes. Geometric wear was analysed by determining changes in the thickness of the brake pad lining during friction tests. In order to determine changes in mass, the brake pads were weighed before and after the test. Brake pad wear was evaluated under dust-free conditions and under exposure to silica dust. The tests revealed significant differences in brake pad wear under dust-free conditions and under exposure to silica dust. Mass loss of brake pad lining at different silica concentrations in airborne dust was described.

Słowa kluczowe: okładziny hamulcowe, zużycie, zapylenie.

Streszczenie: W pracy przedstawiono wyniki pomiarów zużycia okładzin hamulców tarczowych w zapyleniu pyłu kwarcowego. W celu przeprowadzenia badań zbudowano nowatorskie stanowisko do badania zużycia okładzin hamulców tarczowych w zapyleniu pyłu kwarcowego. Zużycie określono metodą geometryczną i wagową. Pomiary w przypadku wyznaczenia zużycia geometrycznego polegały na ocenie zmian grubości okładziny hamulcowej podczas prób tarcia. W przypadku metody wagowej dokonano pomiaru masy klocka hamulcowego przed badaniem oraz po wykonaniu badania. Badania zużycia klocków hamulcowych dokonano w warunkach środowiska bez zapylenia oraz w zapyleniu pyłem kwarcowym. Przeprowadzone wyniki badań wykazały istotne różnice w procesie zużywania klocków hamulcowych pomiędzy próbami wykonywanymi bez zapylenia, a tymi wykonywanymi w zapyleniu. Przedstawiono przebieg ubytku masowego w zależności od stopnia zapylenia powietrza kwarcem.

INTRODUCTION

Brake pads are an important component of a vehicle's braking system. Brake pads should be made of materials characterised by high durability, stable frictional properties, and high resistance to wear under various loads, driving speeds, temperatures, and environmental conditions. The choice of suitable materials for the production of brake pads has been researched extensively by both automotive engineers and academic centres, and considerable research has been done on materials with unique abrasive properties. Pinca-Bretotean et al. **[L. 1]** described a new type of abrasive material made of coconut fibre and solid lubricant modifiers produced with the use of a powder metallurgy technique. Materials with the required abrasive properties are selected by analysing their wear **[L. 2]**. The cited study examined three brake pad types: a real automotive pad and two composite

[*] ORCID: 0000-0002-8218-1540. The University of Warmia and Mazury in Olsztyn, Department of Vehicle and Machine Design and Operation, M. Oczapowskiego 11 Street, 10-719 Olsztyn, Poland, e-mail: piotr.szczyglak@uwm.edu.pl.
[**] ORCID: 0000-0003-2953-7402. The University of Warmia and Mazury in Olsztyn, Department of Vehicle and Machine Design and Operation, M. Oczapowskiego 11 Street, 10-719 Olsztyn, Poland, e-mail: jerzy.napiorkowski@uwm.edu.pl.
[***] The University of Warmia and Mazury in Olsztyn, M. Oczapowskiego 11 Street, 10-719 Olsztyn, Poland, e-mail: mateusz.sydorczyk@student.uwm.edu.pl.

formulations. The composite containing graphite lubricant was characterised by optimal frictional properties and the highest resistance to wear. Surface profilometry is also a useful technique for evaluating brake pad wear **[L. 3]**. The cited authors analysed the operation of a brake disc/brake pad friction pair under normal and difficult driving conditions in an urban environment. The results of the profilometry analysis proved to be highly useful for assessing brake wear. Deep grooves on a brake disc operated under difficult driving conditions was attributed to fouling or the presence of a foreign body between the brake pad and the brake disc. In addition to materials, the frictional properties of brake pads are also affected by operating conditions **[L. 4]**. Świderski et al. **[L. 5]** demonstrated that the wear of brake system components is also significantly influenced by the type of driving environment and season of the year. Brake wear was significantly higher in the summer (high temperature) and urban driving environments.

Machines and vehicles are operated under various environmental conditions. Based on their origin, particulate matter emissions from vehicular traffic and machine operations can be divided into two categories: exhaust gas particles and particles that are generated by non-exhaust (environmental) sources and become resuspended due to traffic-induced turbulence **[L. 6]**. In vehicles and machines operated on dusty field roads and unpaved roads, various contaminants can be deposited between brake system components. Polydisperse dust suspended in the air can compromise the performance and durability of vehicles and machines. Dust is composed of variously sized particles **[L. 7]**:

- below 1 μm – invisible to the naked eye,
- 2–10 μm – suspended in the air for relatively long periods of time,
- 10 – 50 μm – most dust particles fall in this size range,
- above 50 μm – dust particles generated during field works, road construction, and in military training grounds.

Silica dust, also known as road dust, contains mainly silicon dioxide (SiO_2). Silicon dioxide content in silica dust usually ranges from 66% to 92% on a mass basis. The damaging effects of silica dust can be attributed to its considerable hardness (7 on the Mohs scale) and geometric properties. Most silica particles are solid objects with an irregular geometric shape, sharp edges and vertices **[L. 8]**. Road dust also contains corundum (aluminium oxide Al_2O_3; up to 13.7% on a mass basis), iron oxide (Fe_2O_3; up to 11%), and calcium oxide (CaO; up to 6.8%). In addition to the chemical composition of mineral dust, the following factors also contribute to brake wear:

- humidity,
- driving speed,
- location of the friction pair, such as the wheel arch,
- impact on the soil surface.

Most research on the construction and operation of braking systems focuses on:

- brake lining materials containing metal fibres **[L. 9–13]**;
- alternative brake lining materials (rice husks, palm seed powder, maise husks, crab shell powder) **[L. 14–17]**;
- the effect of temperature on brake pad wear and emissions of toxic particulate matter (road tests involving a brake tester and laboratory tests involving a pin-on-disc machine) **[L. 18–21]**;
- the effect of braking force on brake pad wear and emissions of toxic particulate matter (laboratory tests) **[L. 22–24]**;
- various types of brake pads (NAO, low-metallic and semi-metallic) **[L. 25–26]**;
- the effect of various brake pad materials on brake pad wear and emissions of toxic particulate matter (road tests, laboratory tests, MES) **[L. 27–29]**;
- the effect of friction force on brake pad wear and emissions of toxic particulate matter (laboratory tests, brake tester, MES) **[L. 22, 30–31]**;
- the effect of deceleration on brake pad wear and emissions of toxic particulate matter (laboratory tests, brake tester, road tests) **[L. 32–34]**;
- the impact of humidity on brake pad wear and emissions of toxic particulate matter (laboratory tests, brake tester) **[L. 35–36]**;
- the influence of brake disc quality on disc corrosion **[L. 37]**.

A review of the literature revealed that the impact of airborne dust on brake pad wear has not been investigated to date. This is an important consideration because the Euro 7 standard will introduce additional limits on emissions from brakes and tires for passenger cars and light vans (from 2025) and heavy-duty vehicles (from 2027) **[L. 38]**. In order to fill in this knowledge gap, the present study was undertaken to examine the effect

of road dust (environmental factor) on brake pad wear, thus identifying areas for improvement in heavy-duty vehicles and machines and their parts so as to minimise the negative impact of non-exhaust emissions on the environment.

MATERIALS AND METHODS

This study aimed to evaluate the effect of silica dust on the wear of disc brake pads. The lining of the analysed brake pad was made of JT6500 material (**Fig. 1a**, **Table 1**), and the brake pad was mounted on a solid disc brake made of ZL250 cast iron (**Fig. 1b**).

The study relied on an active experimentation approach. The analysed brake pad is presented in **Figure 2**.

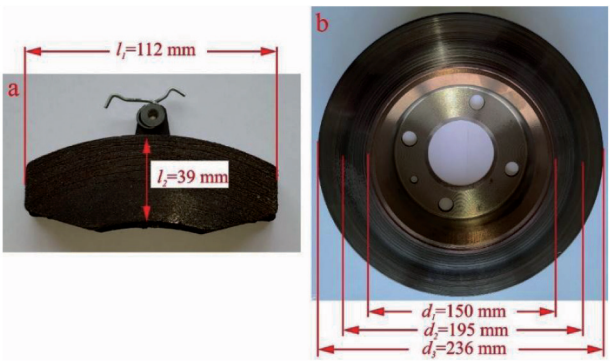

Fig. 1. View of the analysed brake disc and brake pad: a) brake pad, b) brake disc, l_1, l_2 – geometric dimensions of the brake pad, d_1 – inner diameter of the active surface of the brake disc, d_2 – diameter of the disc-pad contact zone, d_3 – outer diameter of the active surface of the brake disc

Rys. 1. Widok tarczy i klocka użytych w czasie badań: a) klocek hamulcowy, b) tarcza hamulcowa, l_1, l_2 – wymiary geometryczne klocka hamulcowego, d_1 – wewnętrzna średnica powierzchni czynnej tarczy, d_2 – średnica poślizgu, d_3 – zewnętrzna średnica powierzchni czynnej tarczy

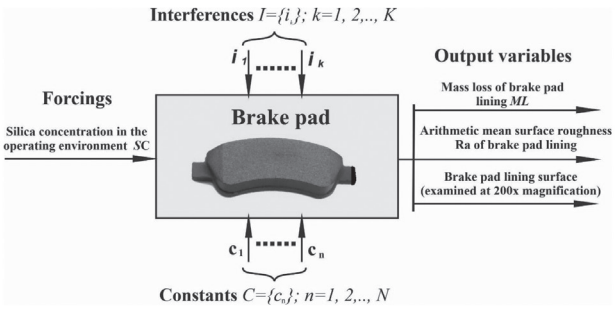

Fig. 2. The analysed brake pad

Rys. 2. Klocek hamulcowy jako przedmiot badań

The abrasive material was silica sand composed of spherical quartz (SiO_2) particles (**Fig. 3**) with 0.1–0.5 mm grain size.

Fig. 3. View of silica sand grains

Rys. 3. Widok ziaren piasku kwarcowego

The following output variables were analysed during the experiment:

- mass loss of brake pad lining ML,
- arithmetic mean surface roughness R_a of brake pad lining,
- brake pad lining surface (examined at 200x magnification).

The following constants were used in the study:

- c_1 – geometric dimensions of brake pad lining (**Fig. 1a**),
- c_2 – geometric dimensions of a solid brake disc (**Fig. 1b**),
- c_3 – active surface of brake pad lining (A = 3828 mm^2),
- c_4 – average diameter of the disc-pad contact zone (d_2 = 195 mm),
- c_5 – rotational speed of the brake disc (n = 1400 rpm),
- c_6 – average sliding velocity (v_p = 4.55 $m \cdot s^{-1}$, i.e., 11% of permissible sliding velocity for JT650 lining),
- c_7 – clamping force (F = 212 N),
- c_8 – pressure per unit area of brake pad lining (p = 55377 Pa),
- c_9 – number of braking cycles (NC = 500),
- c_{10} – duration of a braking cycle (t_c = 30 s, **Fig. 4**),
- c_{11} – braking time (t_h = 10 s, **Fig. 4**),
- c_{12} – operating environment (temperature – 25°C, humidity – 50%).

The following types of wear were observed during the experiment:

- i_1 – wear of passive pad lining, which protects backing plates against corrosion (this problem was eliminated by removing passive lining),
- i_2 – friction-induced wear of backing plates (this problem was minimised by applying lubricant to guide rails and the calliper's components; the lubricant was removed from the pad before weighing).

The physical and mechanical properties of brake pad lining and its operating characteristics are presented in **Table 1**.

Table 1. Physical and mechanical properties of brake pad lining based on the manufacturer's specification [L. 39]
Tabela 1. Właściwości fizyko-mechaniczne okładziny ciernej wg producenta **[L. 39]**

No.	Physical and mechanical properties	Value	Unit of measurement
1	Density at 20° (PN-92/C-82055/10)	2.7	$g \cdot cm^{-3}$
2	Hardness H at 20° (PN-93/C-89030/01)	78	MPa
3	Recommended pressure per unit area	1-6	MPa
4	Recommended sliding velocity	up to 40	$m \cdot s^{-1}$
5	Operating temperature – instantaneous	500	°C
6	Operating temperature – long-term	400	°C
7	Chemical resistance (brake fluid, Diesel oil, petrol, solid and liquid lubricants)	good	–
Lining material:	Asbestos-free, based on synthetic resins, synthetic rubber, metal powder and steel fibre fillers, mineral fibres, friction adjusting and stabilising materials		

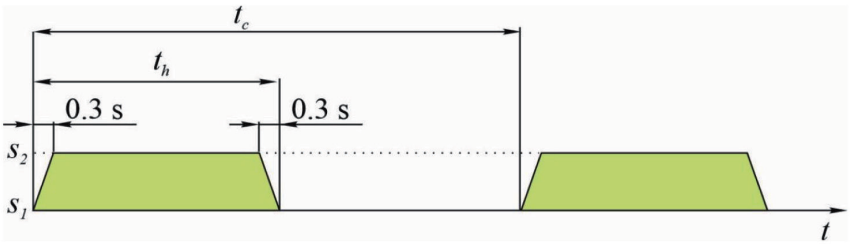

Fig. 4. Braking cycle: t_c – duration of the braking cycle, t_h – braking time, s_1 – stop, s_2 – deceleration
Rys. 4. Schemat przebiegu czasowego procesu hamowania: t_c – czas trwania cyklu, t_h – czas hamowania, s_1 – stan spoczynku, s_2 – stan hamowania

The experiment was conducted on a prototype test bench (**Fig. 5**). The brake disc drive system (**Fig. 5 – 1**) consists of a 3 kW electric motor that drives a shaft with the brake disc via a flexible coupler. The brake was mounted in a chamber (**Fig. 5 – 2**), and a stream of silica sand was fed to the chamber from the sand dosing unit (**Fig. 5 – 3**). The dosing unit was composed of a buffer tank, and sand was fed gravitationally via a dosing valve to the channel in a stream of air generated by the fan. After passing the chamber (**Fig. 5 – 2**), silica sand was captured by the separator (**Fig. 5 – 4**). The test stand was equipped with a control module (**Fig. 5 – 5**).

The analysed brake is presented in **Figure 6**. The brake disc (**Fig. 6 – 2**) with brake pads (**Fig. 6 – 3**) was mounted on the driving shaft (**Fig. 6 – 1**). The calliper (**Fig. 6 – 4**) was controlled by a pneumatic

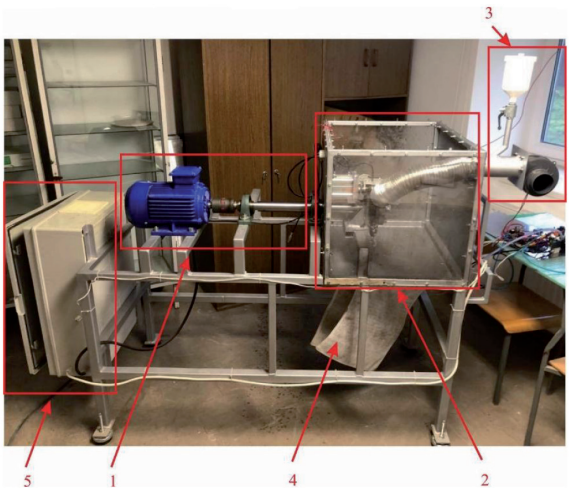

Fig. 5. Prototype test bench: 1 – brake disc drive system, 2 – brake chamber, 3 – sand dosing unit, 4 – sand separator, 5 – control module
Rys. 5. Prototypowe stanowisko badawcze: 1 – układ napędowy tarczy, 2 – komora hamulca, 3 – dozownik piasku, 4 – separator piasku, 5 – moduł sterowania

cylinder (**Fig. 6 – 5**) with a rod diameter of 63 mm. A stream of air with silica sand was fed to the brake with the use of a gear mechanism (**Fig. 6 – 6**). Disc temperature was monitored during the test (50– – 200°C). According to the manufacturer, the wear of the JT6500 brake pad lining is minimised within a temperature range of 50 – 200°C. A temperature sensor (**Fig. 6 – 7**) was installed inside the calliper (**Fig. 6 – 4**). When the disc temperature (estimated by the control system) approximated 200°C, the braking process was paused until the disc cooled to a temperature of 50°C, and then it was continued.

The control system was based on an ATMega2560 microcontroller (**Fig. 1**). The electric motor driving the brake disc (start-stop, changes in disc rotational speed) and the fan generating a stream of air (start-stop) were controlled by the microcontroller via a phase inverter. The microcontroller also indirectly monitored brake disc temperature by reading the signal generated by the temperature sensor in the calliper. The braking process was controlled with the use of a pneumatic cylinder. The microcontroller controlled the movement of the piston rod and the activation of the brake system (start-stop) via two solenoid valves. The pneumatic cylinder control system was equipped with an air compressor and a 1 dm3 buffer tank to ensure smooth operation.

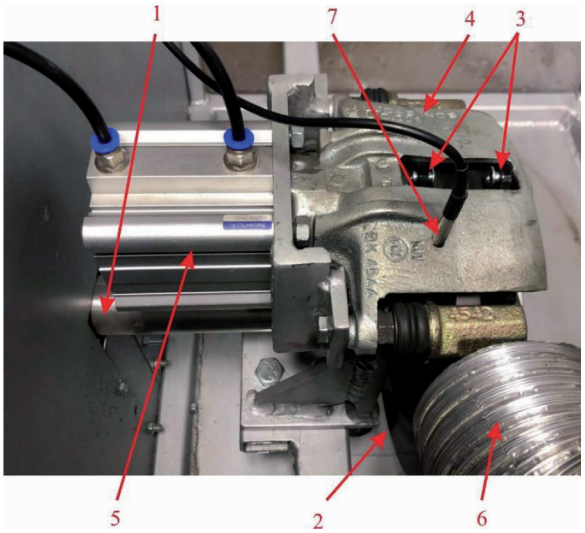

Fig. 6. Brake: 1 – driving shaft of the disc, 2 – disc, 3 – pads, 4 – calliper, 5 – pneumatic cylinder, 6 – gear mechanism for dosing sand, 7 – temperature sensor

Rys. 6. Hamulec: 1 – wał napędowy tarczy, 2 – tarcza, 3 – klocki, 4 – zacisk, 5 – cylinder pneumatyczny, 6 – kierownica zapylonego piaskiem powietrza, 7 – czujnik temperatury

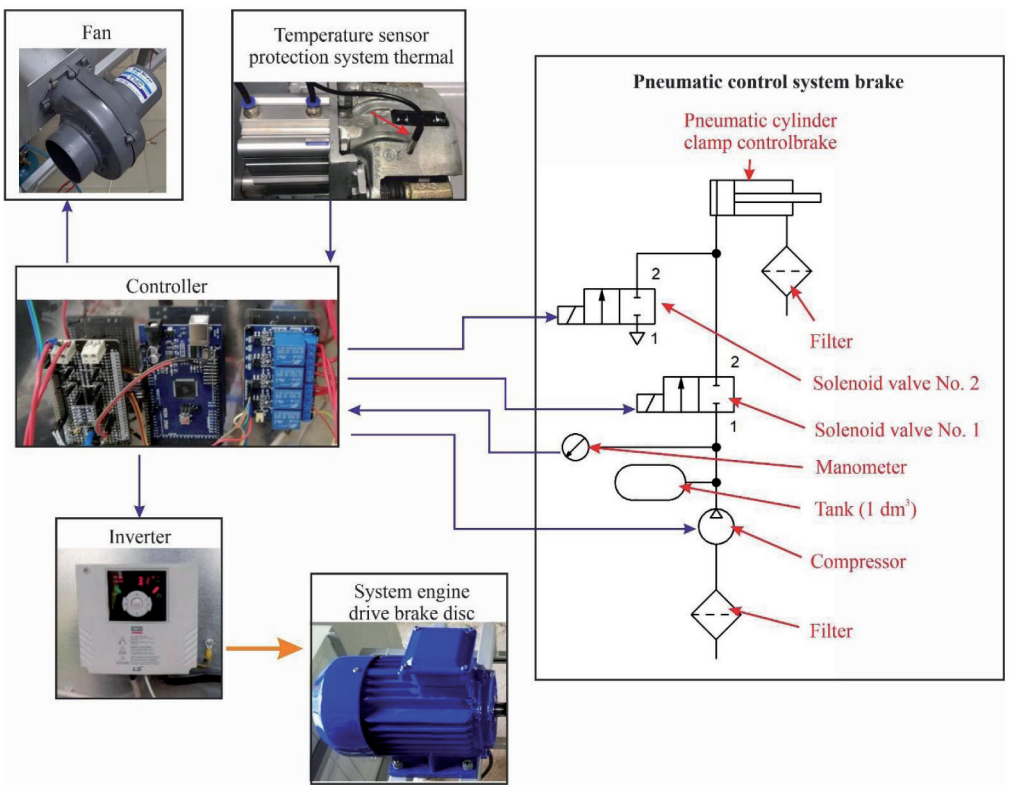

Fig. 7. Diagram of the control system

Rys. 7. Schemat układu sterowania stanowiska badawczego

During the experiment, the mass of brake pads was determined to the nearest 0.001 g with the use of a RADWAG PS 750.R2.H laboratory weighing scale. The arithmetic mean surface roughness *Ra* of the brake pad lining was determined with the Hommel Werke T1000 roughness meter. The surface of the brake pad was examined under the VHX-7000 digital microscope. The experimental design is presented in **Table 2**.

Table 2. Experimental design
Tabela 2. Plan badania

Trial	Cycle duration t_c [s]	Braking time t_h [s]	Number of cycles *NC*	Sliding velocity v_p [m·s^{-1}]	Braking force *F* [N]	Silica concentration *SC* [g·m^{-3}]	Analysed parameters
1	30	10	500	4.55	212	0	Mass loss of brake pad lining *ML*
2							
3						7.91	
4							
5						13.5	Arithmetic mean surface roughness R_a
6							
7						19	
8							
9						31.67	Brake pad lining surface
10							

RESULTS

The mass of the brake pad lining *ML* (arithmetic mean) during the experiment is presented in **Fig. 8**. Brake pad wear increased with a rise in silica concentration *SC* in the operating environment, and the observed relationship was nearly linear (R^2 = 0.96) within a silica concentration of 0–31.67 g·m^{-3}.

Relative mass loss was calculated using the following formula:

$$MLR = \frac{ML - ML(0)}{SC}\left[\frac{g*}{g \cdot m^{-3}}\right] \quad (1)$$

where:
ML – mass loss of brake pad lining [g*],
ML(0) – mass loss of brake pad lining in a dust-free environment [g*],
SC – silica concentration in the operating environment [g·m^{-3}].

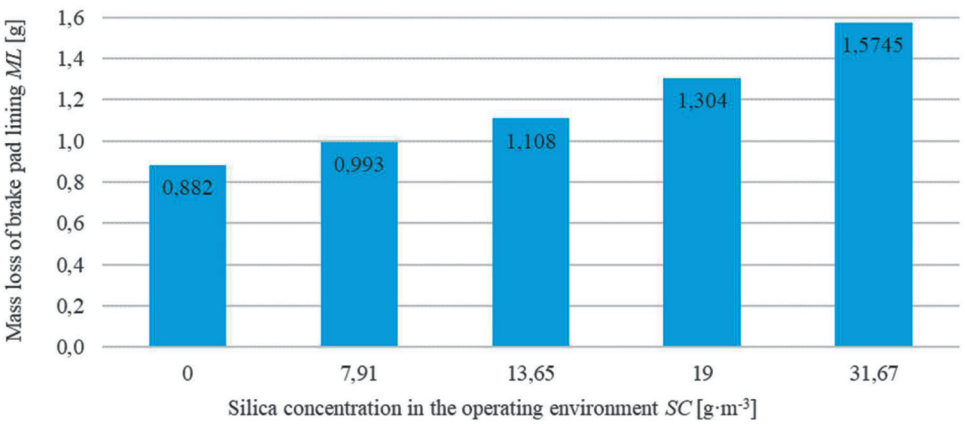

Fig. 8. Mass loss of brake pad lining *ML* at different silica concentrations *SC* in the operating environment
Rys. 8. Zużycie masowe okładziny klocka hamulcowego *ZM* w zależności od natężenia zapylenia piaskiem kwarcowym *NZ*

The calculated relative mass loss of brake pad lining *MLR* is presented in **Figure 9**.

An analysis of the data presented in **Fig. 9** revealed a nearly linear increase ($R^2 = 0.95$) in relative mass loss of brake pad lining *MLR* up to a silica concentration *SC* of 19 g·m^{-3}. This parameter was stabilised at around 0.22 g*·(g·m^{-3})$^{-1}$. Further relative mass loss of brake pad lining was not observed when the concentration of silica particles in the operating environment exceeded 19 g·m^{-3}.

The arithmetic mean surface roughness R_a at different silica concentrations *SC* in the operating environment is presented in **Figure 10**. The roughness of the brake pad lining surface increased

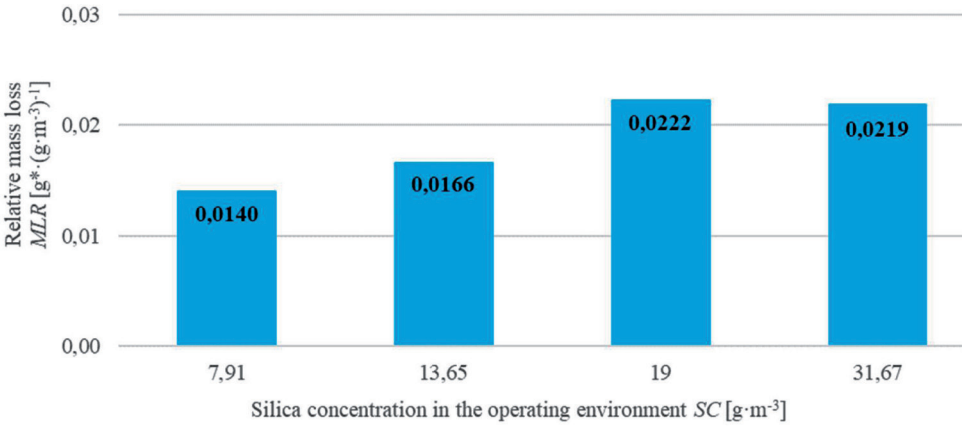

Fig. 9. Relative mass loss of brake pad lining *MLR* at different silica concentrations *SC* in the operating environment
Rys. 9. Względne zużycie masowe okładzin klocka hamulcowego *WM* w zależności od natężenia zapylenia piaskiem kwarcowym *NZ*

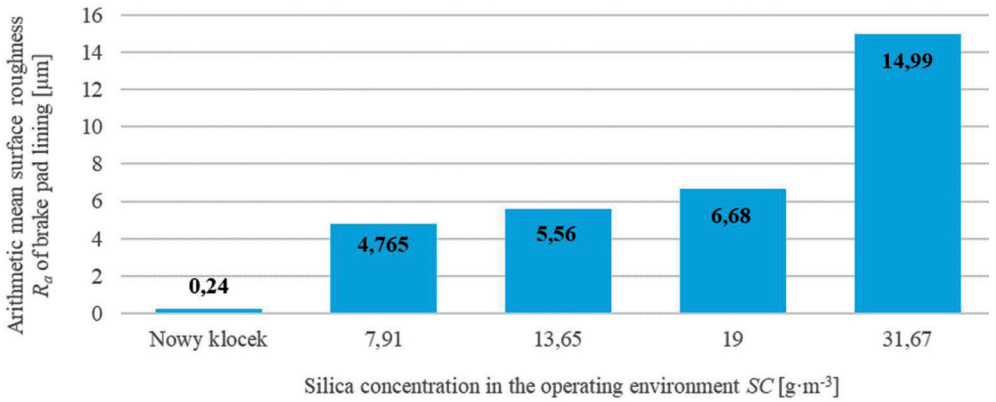

Fig. 10. Arithmetic mean surface roughness R_a at different silica concentrations *SC* in the operating environment
Rys. 10. Średnia arytmetyczna wartości rzędnych profilu R_a w zależności od natężenia zapylenia *NZ*

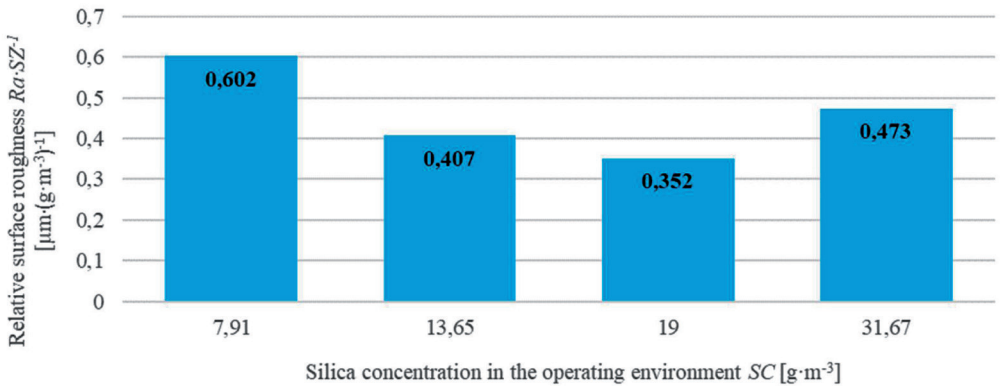

Fig. 11. Relative surface roughness $R_a \cdot SZ^{-1}$
Rys. 11. Względna chropowatość $R_a \cdot NZ^{-1}$

considerably under exposure to higher silica concentrations. The relative surface roughness $R_a \cdot SZ^{-1}$ was also calculated (**Fig. 11**). Relative surface roughness $R_a \cdot SZ^{-1}$ peaked at the lowest silica concentration, which indicates that brake pad lining wear proceeds rapidly already under exposure to low dust levels. The brake pad lining wear rate decreased with a rise in silica concentration *SC*, ranging from 0.351 to 0.473.

A microscopic view of the brake pad lining surface after exposure to different silica concentrations *SC* is presented in **Figure 12**. An increase in silica concentration strongly affected the brake pad lining surface, and the brake pad lining

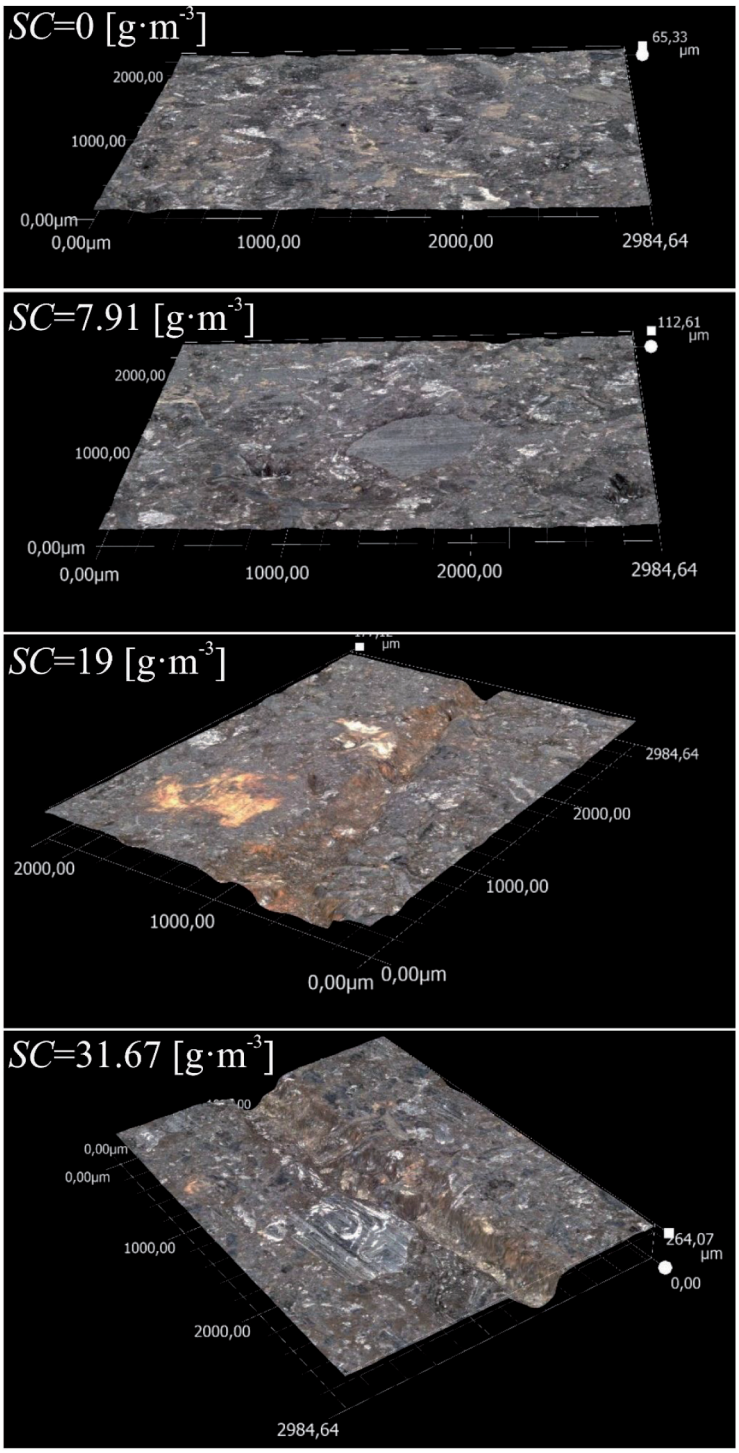

Fig. 12. Microscopic view of the brake pad lining surface at different silica concentrations in the operating environment
Rys. 12. Widok mikroskopowy powierzchni okładzin klocka hamulcowego przy różnych natężeniach zapylenia

wear was uniform when the operating environment was free of silica. Local cavities and grooves were observed under exposure to a silica concentration of 7.91 g·m^{-3}, whereas microgrooves and ridges stretching along the entire active pad lining were noted at a silica concentration of 19 g·m^{-3} and higher (**Fig. 13**).

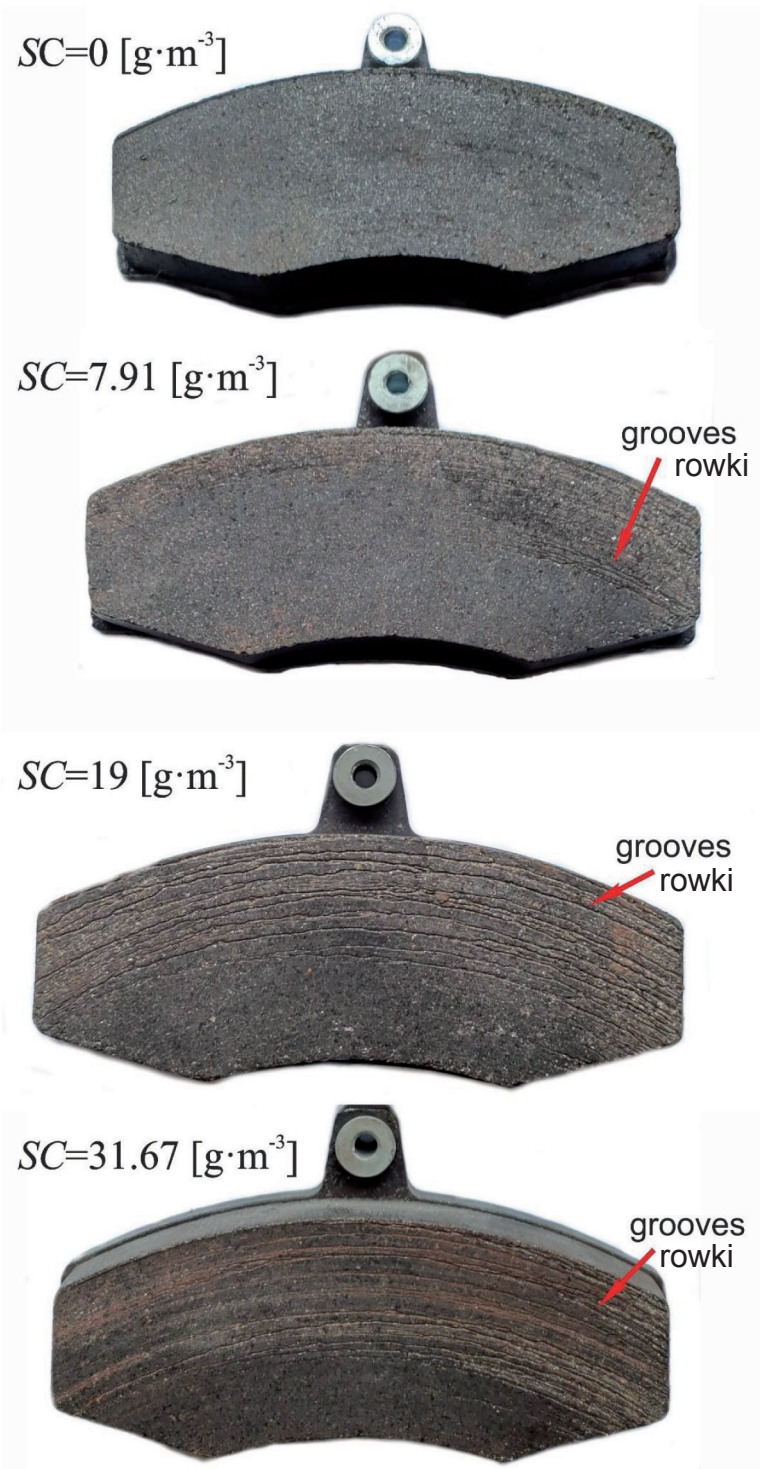

Fig. 13. View of brake pads exposed to different silica concentrations in the operating environment
Rys. 13. Widok klocków hamulcowych w zależności od różnego natężenia zapylenia

CONCLUSIONS

An original test stand for analysing the abrasive wear of brake pad lining was proposed in the study. The wear of the brake pad lining was examined under exposure to different silica concentrations in the operating environment. A review of the literature revealed that the impact of different particulate matter concentrations in airborne dust on brake pad wear has not been researched to date. Brake systems have been analysed under normal environmental (road) conditions by measuring disc and pad temperature during braking, braking distance, deceleration, and braking time **[L. 37, 40]**. However, the cited authors did not analyse the effect of particulate matter concentrations in airborne dust on brake pad wear, and their results cannot be compared with the present findings.

This study demonstrated that silica concentration in the operating environment considerably affects the brake pad wear rate.

The following conclusions can be formulated based on the present findings:

- an increase in silica concentration in the operating environment leads to greater mass loss of brake pad lining *ML*, and the observed relationship is linear;
- even low concentrations of particulate matter in airborne dust cause considerable damage to the brake pad lining surface;
- relative mass loss of the brake pad lining *MLR* increases up to a silica concentration *SC* of 19 $g \cdot m^{-3}$, and parameter *MLR* is stabilised at around 0.22 $g^* \cdot (g \cdot m^{-3})^{-1}$ when silica concentration exceeds the above threshold;
- under exposure to silica concentrations below 19 g·m3, mass loss of brake pad lining is inversely proportional to the clearance between the brake pad lining and the brake disc; the clearance is affected by a small number of large quartz particles which are embedded in the lining under the influence of high braking forces or are broken down, which decreases the clearance and promotes the accumulation of a larger number of small particles between the brake pad lining and the brake disc;
- under exposure to silica concentrations above 19 g·m3, mass loss of the brake pad lining is stabilised due to the accumulation of large quartz particles in the clearance between the brake pad lining and the brake disc; large quartz particles are not broken down or embedded in the lining because the braking force is smaller (distributed over a larger number of particles), which stabilises the clearance, prevents the accumulation of small particles, and, consequently, leads to the formation of microgrooves and ridges;
- the relative surface roughness $R_a \cdot SZ^{-1}$ of the brake pad lining is highest at the lowest concentration of particulate matter, which indicates that under these conditions, brake pad wear proceeds most rapidly per unit of silica concentration in airborne dust.

In the next stage of the study, brake pad wear will be analysed under exposure to different concentrations of other types of particulate matter in road dust (corundum – aluminium oxide Al_2O_3, iron oxide Fe_2O_3, calcium oxide CaO).

REFERENCES

1. Pinca-Bretotean C., Josana A., Birtok-Băneasă C.: Laboratory testing of brake pads made of organic materials intended for small and medium vehicles, IOP Conf. Series: Materials Science and Engineering, 2018, 393, 012029, pp. 1–7.
2. Elzayady, N, Elsoeudy, R. 2021. Microstructure and wear mechanisms investigation on the brake pad. Journal of Materials Search and Technology, 2021, 11, pp. 2314–2335.
3. Marcol D., Stanik Z.: Ocena zużycia awaryjnego pary ciernej klocek–tarcza hamulcowa na podstawie ilościowej i jakościowej analizy metalograficznej oraz badań topografii powierzchni 2d, Autobusy, 2017, 12, pp. 1122–112.
4. Kuliś E., Żółtowski B.: Badania układów hamulcowych, Studies & Proceedings of Polish Association for Knowledge Management, 2011, Nr 47, pp. 126–140.

5. Świderski A., Borucka A., Jacyna-Gołda I., Szczepański E.: Wear of brake system components in various operating conditions of vehicle in the transport company, Maintenance and Reliability, 2019, 21 (1), pp. 1–9.
6. Grigoratos T., Martini G.: Brake wear particle emissions, Environmental Science and Pollution Research, 2015, 22, pp. 2491–2504.
7. Dziubak T.: Operating fluids contaminantions and their effect on the wear of elements of a motor vehicle's combustion engine, The Archives of automotive Engineering, 2016, 72(2), pp. 43–72.
8. Ligier K., Napiórkowski J., Lemecha M.: Effect of Abrasive Soil Mass Grain Size on the Steel Wear Process, Tribology in Industry, 2020, 42(2), pp. 165–176.
9. Grigoratos T., Martini G.: Brake wear particle emissions: a review, Environ Sci Pollut Res, 2015, 22, pp. 2491–2504. DOI 10.1007/s11356-014-3696-8.
10. Ma Y., Martynková G.S., Valášková M., Matějka V., Lu Y.: Effects of $ZrSiO_4$ in non-metallic brake friction materials on friction performance, Tribology International, 2008, 41 (3), pp. 166–174.
11. Banait A.S., Raibhole V.N.: Study on tribological investigations of alternative automotive brake pad materials. In 8th National Conference on Recent Developments in Mechanical Engineering, pp. 40–43.
12. Jadhav S.P., Sawant S.H.: A review paper: Development of novel friction material for vehicle brake pad application to minimize environmental and health issues, Materials Today: Proceedings, 2019, 19, pp. 209–212.
13. Valotto G., Zannoni D., Rampazzo G., Visin F., Formenton G., Gasparello A.: Characterization and preliminary risk assessment of road dust collected in Venice airport (Italy), Journal of Geochemical Exploration, 2018, 190, pp. 142–153.
14. Primaningtyas W.E., Sakura R.R., Syafi'i I., Adhyaksa A.A.G.A.D.: Asbestos-free brake pad using composite polymer strengthened with rice husk powder, In IOP Conference Series: Materials Science and Engineering, 2019, Vol. 462, No. 1, p. 012015, IOP Publishing, 1–6.
15. Pujari S., Srikiran S.: Experimental investigations on wear properties of palm kernel reinforced composites for brake pad applications, Defence Technology, 2019, 15(3), pp. 295–299.
16. Asotah W., Adeleke A.: Development of asbestos free brake pads using corn husks, Leonardo Electronic Journal of Practices and Technologies, 2017, 31, pp. 129–144.
17. Singaravelu D.L., Vijay R., Manoharan S., Kchaou M.: Development and performance evaluation of eco-friendly crab shell powder based brake pads for automotive applications, International Journal of Automotive and Mechanical Engineering, 2019, 16(2), pp. 6502–6523.
18. Alemani M., Wahlström J., Olofsson U.: On the influence of car brake system parameters on particulate matter emissions, Wear, 2018, 396, pp. 67–74.
19. Nosko O., Olofsson U.: Quantification of ultrafine airborne particulate matter generated by the wear of car brake materials, Wear, 2017, 374, pp. 92–96.
20. Zum Hagen F.H.F., Mathissen M., Grabiec T., Hennicke T., Rettig M., Grochowicz J., Benter T.: On-road vehicle measurements of brake wear particle emissions, Atmospheric Environment, 2019, 217, p. 116943.
21. Bonfanti A.: Low-impact friction materials for brake pads (Doctoral dissertation, University of Trento), 2016.
22. Zhang S., Hao Q., Liu Y., Jin L., Ma F., Sha Z., Yang D.: Simulation study on friction and wear law of brake pad in high-power disc brake, Mathematical Problems in Engineering 2019.
23. Gawande S.H., Raibhole V.N., Banait A.S.: Study on tribological investigations of alternative automotive brake pad materials, Journal of Bio-and Tribo-Corrosion, 2020, 6(3), pp. 1–10.
24. Ahmad F., Lo, S.J., Aslam M., Haziq A.: Tribology behaviour of alumina particles reinforced aluminium matrix composites and brake disc materials, Procedia engineering, 2013, 68, pp. 674–680.
25. Wahlström J., Söderberg A., Olander L., Jansson A., Olofsson U.: A pin-on-disc simulation of airborne wear particles from disc brakes, Wear, 2010, 268(5–6), pp. 763–769.
26. Kukutschová J., Roubíček V., Mašláň M., Jančík D., Slovák V., Malachová K., Filip P.: Wear performance and wear debris of semi-metallic automotive brake materials, Wear, 2010, 268(1–2), pp. 86–93.
27. Balakrishnan E., Meganathan S., Balachander M., Ponshanmugakumar A.: Elemental analysis of brake pad using natural fibres, Materials Today: Proceedings, 2019, 16, pp. 1067–1074.

28. Barros L.Y., Poletto J.C., Neis P.D., Ferreira N.F., Pereira C.H.: Influence of copper on automotive brake performance, Wear, 2019, 426, pp. 741–749.
29. Lagel M.C., Hai L., Pizzi A., Basso M.C., Delmotte L., Abdalla S., Al-Marzouki F.M.: Automotive brake pads made with a bioresin matrix, Industrial Crops and Products, 2016, 85, pp. 372–381.
30. Li G., Yan Q., Jianren X., Qi, G, Yang, X.: The stability of the coefficient of friction and wear behavior of C/C–SiC, Tribology Letters, 2015, 58(1), pp. 1–7.
31. Xiao X., Yin Y., Bao J., Lu L., Feng X.: Review on the friction and wear of brake materials, Advances in Mechanical Engineering, 2016, 8(5), 1687814016647300.
32. Hagino H., Oyama M., Sasaki S.: Laboratory testing of airborne brake wear particle emissions using a dynamometer system under urban city driving cycles, Atmospheric Environment, 2016, 131, pp. 269–278.
33. Riediker M., Gasser M., Perrenoud A., Gehr P., Rothen-Rutishauser B.: A system to test the toxicity of brake wear particles, Am J Respir Crit Care Med, 2008, 177(1), pp. 1–23.
34. Neis P.D., Ferreira N.F., Sukumaran J., De Baets P., Ando M., Matozo LT., Masotti D.: Characterization of surface morphology and its correlation with friction performance of brake pads, Sustainable construction & design, 2015, 6(1).
35. Ozcan S., Filip P.: Wear of carbon fiber reinforced carbon matrix composites: Study of abrasive., oxidative wear and influence of humidity, Carbon, 2013, 62, pp. 240–247.
36. Blau P.J., McLaughlin J.C.: Effects of water films and sliding speed on the frictional behavior of truck disc brake materials, Tribology international, 2003, 36(10), pp. 709–715.
37. Synák F., Jakubovičová L., Klačko M.: Impact of the choice of available brake discs and brake pads at different prices on selected vehicle features, Appl. Sci., 2022, 12 7325, pp. 0–32, https://doi.org/10.3390/app12147325.
38. https://www.auto-swiat.pl/wiadomosci/aktualnosci/nowa-norma-emisji-spalin-euro-7-czyli-wojna-o-przepisy-i-przyszlosc-samochodow/c4cdq91
39. Makland. 2015. Materiał JT6500 i test zużyciowy materiał cierny: JT6500.
40. Viderščak D., Schauperl Z., Ormuž K., Šolić S., Nikšić M., Milčić D., Ormuž P.: Influence of brake pad propertiesto braking characteristics, Promet–Traffic&Transportation, 2022, Vol. 34, No. 1, pp. 91–102, DOI: https://doi.org/10.7307/ptt.v34i1.3846.